J Mater Sci (2007) 42:2175–2180
DOI 10.1007/s10853-006-1058-8

Compositional analysis and electrical properties of Sb, Mn-doped barium strontium titanate PTCR ceramics with TiO_2 and SiO_2 sintering additives

P. Bomlai · N. Sirikulrat · A. Brown · E. Condliffe · S. J. Milne

Received: 18 May 2005 / Accepted: 9 January 2006 / Published online: 24 February 2007

Abstract The secondary phase compositions in Sb-doped (Ba, Sr)TiO_3 ceramics containing SiO_2 and excess TiO_2 sintering additives have been examined by XRD, BEI and EPMA techniques. It is shown that alongside the primary $(Ba_{0.797}Sr_{0.2}Sb_{0.003})TiO_3$ phase, $(Ba_{1.95}Sr_{0.05})_2(Ti_{1.2}Si_{1.8})O_8$ and Sb-doped $(Ba_{0.99}Sr_{0.01})_6Ti_{17}O_{40}$ phases form at the intergranular regions. Substitution of up to 0.04 mol% MnO_2 enhances the PTCR effect, giving a ratio $\rho_{max}/\rho_{min} \sim 7 \times 10^5$ for the optimum 0.04% MnO_2 composition. At this level Mn cannot be detected in the microstructure by EPMA, however in insulating samples containing 0.08 mol% of MnO_2, it was detected in the $(Ba_{0.99}Sr_{0.01})_6Ti_{17}O_{40}$ intergranular phase.

Introduction

Donor-doped barium titanate ($BaTiO_3$) ceramics that exhibit a positive temperature coefficient of resistivity (PTCR) are widely used in many applications including current limiters, motor protection devices, heating elements, and thermal controllers [1–3]. The PTCR effect refers to a nonlinear change in a material's resistivity with temperature, and occurs around its ferroelectric Curie temperature (T_C). The T_C of $BaTiO_3$ can be shifted to lower temperatures by substituting barium with strontium such that a barium strontium titanate ($Ba_{1-x}Sr_xTiO_3$) solid solution forms [4–5]. Additionally it has been established that small additions of some 3d-transition metal elements (and in particular Mn) considerably enhance the PTCR effect [6].

Heywang first proposed that the PTCR effect in semiconducting ceramics was dependent on electron traps (acceptor states) along grain boundaries resulting in electron depletion layers and Schottky barriers [7]. Jonker subsequently explained the absence of any PTCR effect below the Curie temperature (T_C) in terms of spontaneous polarisation of ferroelectric domains [8]. The overall resistance of the sample is dependent on the resistance of the grain boundary regions, the value being affected by interaction with oxygen and changes to the density of acceptor states during processing. A maximum resistance is reached at T_{max}, due to the increasing energy levels of electron traps.

To simplify the processing of $BaTiO_3$ ceramics, an excess of TiO_2 and SiO_2 have often been used as sintering additives in order to create a liquid phase that reduces the sintering temperature and helps control the microstructure. It is noted that an excess of TiO_2 forms the well-known eutectic $BaTiO_3$-$Ba_6Ti_{17}O_{40}$ at 1320–1332°C [9–10]. Co-additions of SiO_2 reportedly produce the secondary crystalline phases $Ba_2TiSi_2O_8$

P. Bomlai (✉)
Materials Science Program, Faculty of Science, Prince of Songkla University, Songkhla 90112, Thailand
e-mail: ppornsuda@yahoo.com

N. Sirikulrat
Department of Physics, Faculty of Science, Chiang Mai University, Chiang Mai 50200, Thailand

A. Brown · S. J. Milne
Institute for Materials Research, University of Leeds, Leeds LS2 9JT, UK

E. Condliffe
School of Earth and Environment, University of Leeds, Leeds LS2 9JT, UK

(fresnoite) and $Ba_6Ti_{17}O_{40}$ in bodies sintered at 1260°C [10–11]. Investigation (by electron microprobe analysis) into the composition of the second phases formed in the BaO : TiO_2 : SiO_2 system was first reported by West et al. [12]. They showed that the major second phase formed is fresnoite-like and has the formula $Ba_2Ti_{1+x}Si_{2-x}O_8$ ($0 \le x \le 0.14$).

The main objective of this work is to confirm the compositions of secondary phases in a barium strontium titanate ceramic doped with Sb_2O_3 and a combination of excess TiO_2 and SiO_2 sintering additives. The Sb_2O_3 acts principally as a donor dopant therefore BST becomes semiconducting and shows PTCR characteristics. A secondary objective is to confirm an enhancement of the PTCR effect in this specific BST –based composition by further doping with MnO_2.

Experimental procedure

Ceramic samples were prepared by the conventional mixed oxide process. The following starting materials of $BaCO_3$, TiO_2, $SrCO_3$, Sb_2O_3, SiO_2 (Aldrich chemical company, Inc., 99.9+ % purity) were used. Target compositions of $(Ba_{0.797}Sr_{0.2})Sb_{0.003}TiO_3$ + 1 mol% TiO_2 + 3 mol% SiO_2 were systematically prepared and are labeled here as Mn-free specimens; Sb^{3+} substitution on Ba^{2+} sites is assumed. The mixed powders were ball-milled with zirconia grinding media in isopropanol for 20 hours, then dried and sieved, followed by calcination at 1000 °C for 3 hours in an alumina crucible, using heating and cooling rates of 5 °C/min. The calcined powders were blended with 1 % PVA binder, and ball-milled for 6 hours, dried and sieved again before pressing into 1.5 cm diameter pellets at 100 MPa. For samples with Mn additions (labeled as Mn-doped) the target calcined powders were mixed with additional MnO_2 to produce compositions in the range 0.005–0.08 mol %. Doped powders were then ball-milled for 20 hours before blending with PVA for pressing. For binder removal, both types of samples were heated at a rate of 2 °C/min, and held at 500 °C for 1 hour. The samples were then sintered in air at 1300 °C or 1350 °C for 1 hour, using heating and cooling rates of 5 °C/min.

Room temperature phase identification of sintered samples was undertaken by the X-ray powder diffraction technique with a scan speed of 0.004 deg s^{-1}, using CuKα radiation (Philips APD1700). Lattice parameters were calculated by using a least squares refinement method [13]. Backscattered electron imaging (BEI) was used to monitor the distributions of each phase in the microstructure (Camscan series 4 SEM, with Oxford Instruments UTW EDX detector/ ISIS software series 300) Specimens were prepared for BEI by polishing resin-mounted specimens, with a final polish using 1 μm diamond paste.

The chemical composition of the sintered bodies was analysed by electron probe microanalysis (EPMA - Cameca Instrument SX50). Fully quantitative analyses were performed using an electron accelerating voltage of 20 kV and a beam current 50 nA. To overcome the problem of overlap of Ba L_α and Ti K_α X-ray lines, the lower counting, higher resolution, LIF (rather than the PET) X-ray detection crystal was used. Well characterized pure $BaTiO_3$ was used as the standard for both Ba and Ti. Correction for inter-elemental effects was by Cameca proprietary phi-rho-z software. The phase compositions determined by EPMA were subsequently compared to those of the 'known' phases, as identified by X-ray diffraction.

The d.c. resistivity change of the samples as a function of temperature, from room temperature to about 300°C were measured using a digital multimeter (Agilent 34401A) and a suitable power supply, after both sides of the specimens had been coated with silver paste.

Results and Discussion

X-ray diffraction patterns of a sintered Mn-free, and a Mn-doped Sb-BST sample are shown in Fig. 1. The major Bragg peaks corresponding to the predominant tetragonal barium strontium titanate (BST) phase are indexed; not shown here is the tetragonal peak splitting that is evident at higher 2θ angles, up to 90°, which was used to calculate lattice parameters [14–15]. The Mn-doped samples showed indistinguishable XRD patterns; estimated lattice parameters of the BST phase in all cases were $a = 3.972 \pm 0.001$ Å and $c = 3.996 \pm 0.003$ Å, giving a c/a ratio of 1.006 ± 0.003.

Numerous faint extra XRD peaks are also evident in Fig 1. Comparison with standard (JCPDS) XRD data files identifies these phases to have $Ba_6Ti_{17}O_{40}$ [16] and $Ba_2TiSi_2O_8$ [17] type structures; peaks of the latter were more intense. The $Ba_6Ti_{17}O_{40}$ –type phase will be referred to as the T phase, while the $Ba_2TiSi_2O_8$ –type phase will be referred to as the S phase.

Backscattered SEM imaging was undertaken on well-polished surfaces of the sintered samples, with and without Mn additions. Different phases are distinguished by their different contrasts in Fig 2. The most dominant phase has the lightest grey contrast, it is clearly present throughout the structure and so can be attributed to the matrix Sb-BST phase [15] revealing a

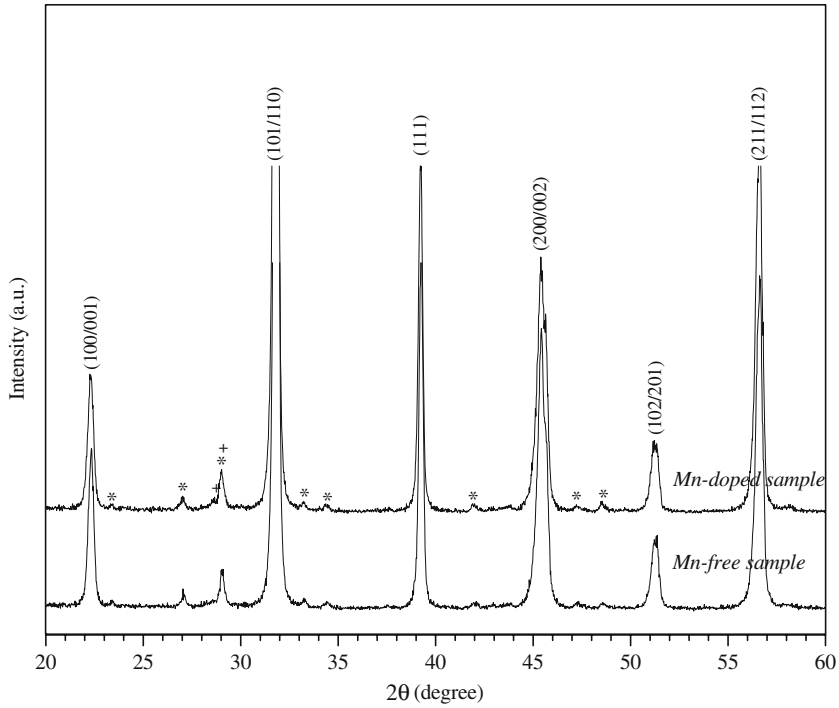

Fig. 1 X-ray diffraction pattern of Mn-free sample sintered at 1300°C and Mn-doped sample sintered at 1350°C showing phase formation (* : $Ba_2TiSi_2O_8$ and + : $Ba_6Ti_{17}O_{40}$)

grain size range of ~ 5 – 25 μm in each sample. The average grain size of the matrix does not alter across the compositional range studied 0–0.08 mol% MnO_2; however higher levels of Mn doping are known to suppress secondary grain growth in titanate perovskite ceramics [18–19]. The second BEI contrast component has black contrast and may be attributed to pores in the sintered body. There is no significant difference in porosity between the Mn-doped and Mn-free specimens. The third and fourth BEI phases can be seen at the grain interfaces of the matrix BST phase and could be distinguished in the original micrographs as mid and dark grey respectively. Due to the atomic number contrast in backscattered electron images the brighter of the two intergranular regions should correspond to the phase containing proportionately more of the higher atomic number element, Ba, *viz.* phase S, whereas the darker regions should be the phase containing more of the lighter Ti, phase T as identified by XRD (see labels in Fig. 2).

Quantitative compositional analyses of the three different sintered solid phases seen in the BE images (Figure 2), as carried out using EPMA, are shown in Table 1 (for a Mn-free sample). The elemental analysis (atomic %) of each of the three phases is an average of 10 point analyses with their corresponding standard deviation shown. The estimated composition of the matrix is consistent with the expected composition of the Sb-BST phase, $(Ba_{0.797}Sr_{0.2}Sb_{0.003})TiO_3$,

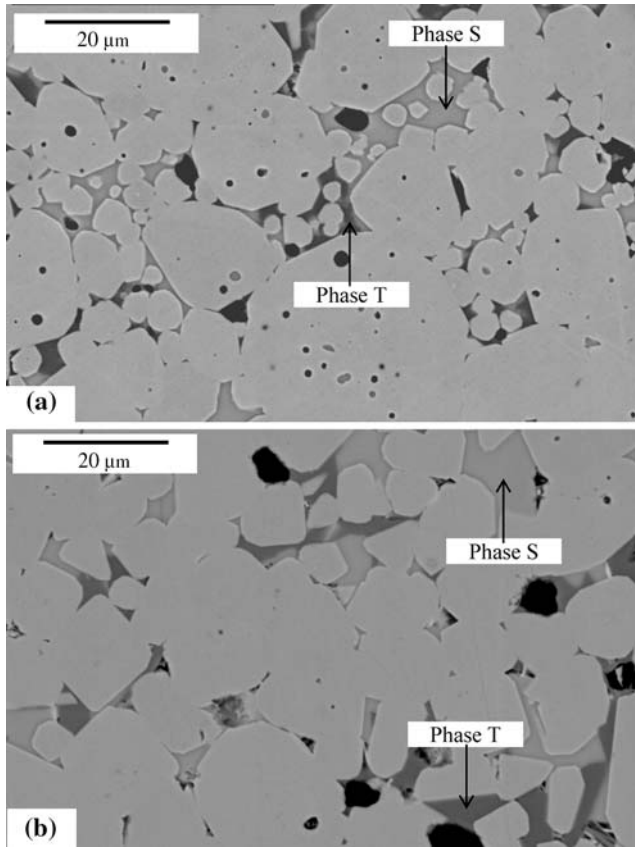

Fig. 2 Backscattered electron image (BEI) of polished samples: (a) Mn- free specimen sintered at 1300 °C; (b) 0.08 mol% Mn doped- specimen sintered at 1350°C

Table 1 Average results of EPMA quantitative analysis of Mn-free specimen

Sample	Composition (Atomic %)				
	Ba	Ti	Sr	Si	Sb
% Theoretical atomic of $(Ba_{0.797}Sr_{0.2}Sb_{0.003})TiO_3$	39.85	50.0	10.0	-	0.15
% Theoretical atomic of $Ba_6Ti_{17}O_{40}$	26.1	73.9	-	-	-
% Theoretical atomic of $Ba_2TiSi_2O_8$	40.0	20.0	-	40.0	-
Sb-BST + TiO_2/SiO_2:					
Matrix grain	39.8 ± 0.2	49.5 ± 0.2	10.5 ± 0.2	0.006 ± 0.004	0.17 ± 0.01
Secondary phase S	38.9 ± 0.2	24.3 ± 1.2	1.1 ± 0.5	35.7 ± 1.0	0.0
Secondary phase T	26.3 ± 0.2	73.2 ± 0.1	0.31 ± 0.02	0.07 ± 0.02	0.088 ± 0.002

notwithstanding the possible effects of beam overlap with the secondary phases. Phase T gave a (Ba + Sr) : Ti ratio of 6.1 : 16.8 which suggests this phase is indeed (Ba, Sr)$_6$Ti$_{17}$O$_{40}$, as suggested by XRD data. The analysed Sr content infers a solid solution composition: $(Ba_{1-x}Sr_x)_6Ti_{17}O_{40}$ with x ~ 0.01 . However antimony was also detected, at a level corresponding to a Sb/(Ba + Sr) ratio of 0.003. In a study of phase equilibria in the $BaTiO_3$-$SrTiO_3$-TiO_2 system, Lee et al. [20] have reported a maximum Sr/(Ba + Sr) ratio of 0.02 which is twice the value found in phase T. Hence our results suggest that for the base composition, $(Ba_{0.797}Sr_{0.2}Sb_{0.003})TiO_3$ with 1 mol % excess TiO_2 (and 3 mol % SiO_2), a $(Ba_{1-x}Sr_x)Ti_{17}O_{40}$ solid solution of intermediate composition (x ~ 0.01), coexists alongside the BST matrix phase. Because of the silica addition, another phase was also present.

For Phase S, EPMA confirmed that the Si content was lower, and Ti content higher, than in fresnoite $Ba_2TiSi_2O_8$. Repeated analysis gave a (Ba + Sr) : Ti : Si elemental ratio of approximately 2 : 1.2 : 1.8. Strontium was also detected. Phase S is therefore identified to be a solid solution: $(Ba_{1-x}Sr_x)_2(Ti_{1+y},Si_{2-y})O_8$, with x ~ 0.005 and y ~ 0.2. It is the Sr substituted analogue of the phase identified by West et al. in SiO_2 modified $BaTiO_3$, namely $Ba_2Ti_{1+y}Si_{2-y}O_8$, for which their limiting composition was y = 0.14 [12]. In the Sr analogue the present data implies a slightly greater range of Ti^{4+} substitution on Si^{4+} sites. No Sb substitution was evident in phase S.

Manganese could not be detected in the BST matrix for any samples made with ≤ 0.04 mol% MnO_2. The analysis data for the other constituent elements was consistent with the phases identified by EPMA in Mn-free samples. A sample containing 0.8 mol % MnO_2 was prepared to investigate if Mn could be detected at this higher concentration. In fact Mn was detected, but only in phase T, the intergranular secondary phase, (Ba, Sr)$_6$Ti$_{17}$O$_{40}$, which revealed 0.03 atom % Mn. BEI images did not show any contrast variations that would have suggested a another discrete intergranular phase, rich in Mn to be present. Therefore, the analysis results suggest that excess Mn ions, beyond an assumed BST-MnO_2 solid solution limit, segregate to, and react with phase T, possibly involving a Ti ion substitution mechanism. The amount of intergranular T phase could not be quantified and so no conclusions can be drawn as to the actual MnO_2-BST solid solution limit or the amount of 'excess' Mn in the sample.

The PTCR characteristics for Mn-free and MnO_2-doped specimens are illustrated by the ρ-T plots shown in Figure 3. Additions of MnO_2 progressively increased the room-temperature resistivity from 48 to 911 Ω cm and increased ρ_{max} by two to three orders of magnitude. Consequently the ratio ρ_{max}/ρ_{min} increased from

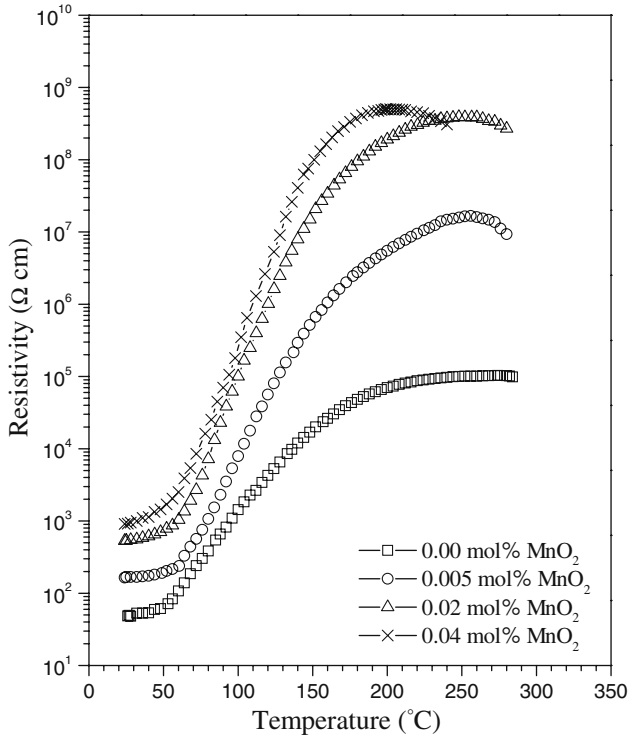

Fig. 3 The resistivity-temperature characteristics of specimens with various MnO_2 contents; (Mn-free specimen sintered at 1300°C, Mn- doped specimens sintered at 1350°C)

Table 2 Summary of electrical data for samples with various amounts of MnO_2 : room temperature resistivity (ρ_{min}), maximum resistivity (ρ_{max}), the resistivity change (ρ_{max}/ρ_{min}), the temperature corresponding to ρ_{max} (T_{max}) as a function of an amount of MnO_2

Specimens with various amounts of MnO_2 (mol %)	ρ_{RT} (Ω cm)	ρ_{max} (Ω cm)	ρ_{max}/ρ_{min}	Tmax (°C)
0.00	48	1.03×105	2.14×10^3	275
0.005	164	1.67×10^7	1.02×10^5	256
0.02	531	3.91×10^8	7.36×10^5	248
0.04	911	5.01×10^8	5.50×10^5	202

~2×10^3 for Mn-free samples up to ~7×10^5 for 0.04 mol% MnO_2 compositions. Values of these parameters are listed in Table 2, together with values of T_{max}, the temperature of maximum resistivity, which decreased with additions of MnO_2. On increasing the Mn content from 0.04 to 0.08 mol% MnO_2 the PTCR semiconducting character disappeared and the samples became insulating.

In Sb-BST, semiconducting grain interiors form by substitution of donor Sb^{3+} on Ba^{2+} and Sr^{2+} sites. Any Sb^{5+} ions which are present may substitute for Ti^{4+}, again acting as a donor [21]. The Sb^{3+} ions may have dual behaviour, also acting as an acceptor creating oxygen vacancies by substitution on Ti^{4+} sites [21]. There are conflicting reports in the literature on the location, oxidation state and role of Mn in doped titanate perovskites [22–25]. The two-step powder synthesis procedures adopted for the Sb, Mn co-doped samples is expected to give rise to powders and ceramics in which Mn species are mainly located at grain boundaries and near grain surfaces. The enhanced PTCR results for the manganese co-doped samples, Fig 3, are consistent with Mn^{2+} or Mn^{3+} ions substituting for Ti^{4+} ions, for example:

$$MnO + \frac{1}{2}O_2 \rightarrow Mn_{Ti} + 2O_o^x + 2h^{\bullet} \quad (1)$$

This increases the number density of acceptor defects at the grain boundary layers, resulting in increased electron traps and higher Schottky barriers to electrical conduction. According to the Heywang model [7,26], the barrier height$^-$ is given by:

$$\phi_0 = \frac{eN_s^2(T)}{8\varepsilon_0\varepsilon_{gb}(T)N_d} \quad (2)$$

Where N_s is the density of trapped electrons at the grain boundaries, N_d is the charge carrier concentration, e is the electron charge, ε_0, is the permittivity in free space, and ε_{gb} is the relative permittivity of grain boundary region.

From Equation (1) the Mn acceptor increases the charge density of trapped electrons, in turn increasing the barrier height,- in equation (2). The resistivity of the sample (ρ) is related to the potential barrier by:

$$\rho = A \exp\left(\frac{e\phi_0}{kT}\right) \quad (3)$$

Where A is a constant and only slightly dependent on the temperature compared with the exponential term, and k is the Bolzmann constant.

Hence the addition of the Mn acceptor dopant causes a more rapid rise in resistivity with temperature as it depends exponentially on the potential barrier height (Equation 3) [27]. This accounts for the experimentally observed steeper increase in resistance for Mn-doped samples shown in Fig 3 (any changes in broadening of the Curie peaks are unlikely to have a strong bearing on the resistivity plots [28–29]. With Mn-doping the resistivity plot showed a ρ_{max} value of ~ 5×10^8 ohm cm, over 3-orders of magnitude higher than the Mn-free samples, which showed a lower, flatter response, Fig 3. The higher ρ_{RT} of Mn doped PTCR samples is consistent with the formation of more resistive grain boundary layers [6]. The higher acceptor state density gives higher measured ρ_{max} and lower T_{max} values as shown in Fig. 3. On the other hand because Mn-free samples possess a lower acceptor state density, they have lower ρ_{max} values and a more 'diffuse' ρ-T response. In samples with higher levels of Mn doping, 0.08 mol %, the acceptor concentration reaches a point where it fully compensates for the Sb donor induced semiconductivity and the samples become insulating, therefore the PTCR effect disappears. In these 0.08 mol % Mn samples it was found that Mn was segregated in the intergranular phase, $(Ba,Sr)Ti_{17}O_{40}$. It has been reported previously that for $BaTiO_3$ ceramics, doping with 0.04 mol% doped $BaTiO_3$ produces a ρ_{max}/ρ_{min} ratio $\leq 3 \times 10^4$ [30–31]. The highest ratio, ~1×10^6, was achieved for a $BaTiO_3$ sample doped with 0.13 mol % Mn [3]. These values are also dependent on parameters such as choice of starting materials, and fabrication conditions. The PTCR values our Sb doped BST, processed with TiO_2 and SiO_2 additives, compare favourably to those of other PTCR compositions, Table 2.

Conclusions

The secondary phases in Sb-doped $(Ba,Sr)TiO_3$ ceramics containing 1 mol% excess TiO_2 and 3 mol% SiO_2 sintering additives were investigated. The results

of electron probe microanalysis showed that an Sb-doped $(Ba_{0.99}Sr_{0.01})_6Ti_{17}O_{40}$ phase and a fresnoite-type phase, $(Ba_{1.95}Sr_{0.05})_2(Ti_{1.2}Si_{1.8})O_8$ formed at intergranular regions in all samples. Additions of MnO_2 beyond the BST-MnO_2 solid solution limit segregated to the $(Ba_{0.99}Sr_{0.01})_6Ti_{17}O_{40}$ intergranular phase. The addition of up to 0.04 mol% MnO_2 resulted in an increased ρ_{max}/ρ_{min} ratio of ~7×10^5, and a lower T_{max} but had no significant effect on the average grain size.

Acknowledgements The authors would like to express their sincere thanks to Tim Comyn, Steve McBride, P Vogel and other IMR colleagues for advice and practical support.

References

1. Lee J-K, Park J-S, Hong K-S, Ko K-H, Lee B-C (2002) J Am Ceram Soc 85:1173
2. Saburi O, Wakino K (1963), IEEE Trans Compon Parts CP-10:53
3. Buchanan RC (1991) In: Ceramic materials for electronics: processing, properties, and applications. Marcel Dekker Inc., New York, p 249
4. Zhao J, Li L, Gui Z (2001) Sens Actuators 95:46
5. Kim J-G, Cho W-S, Park K (2001) Mater Sci Eng B 83:123
6. Al-Allak HM, Brinkman AW, Russell GJ, Woods J (1988) J Appl Phys 63:4530
7. Hewang W (1964) J Am Ceram Soc 47:484
8. Jonker GH (1964) Solid State Electron 8:895
9. Yoo Y-S, Kim H, Kim D-Y (1997) J Eur Ceram Soc 17:805
10. Felgner K-H, Müller T, Langhammer HT, Abicht H-P (2001) J Eur Ceram Soc 21:1657
11. Senz S, Graff A, Blum W, Hesse D (1998) J Am Ceram Soc 81:1317
12. Coats AM, Hirose N, Marr J, West AR (1996) J Sol State Chem 126:105
13. Cullity BD, Stock SR (2001) In: Elements of X-ray diffraction. Prentice Hall, New Jersey, p 295
14. Joint Committee for Powder Diffraction standard, Card No. 44-0093
15. Bomlai P, Sirikulrat N, Brown A, Milne SJ (2005) J Eur Ceram Soc 25:1905
16. Joint Committee for Powder Diffraction standard, Card No. 77-1566
17. Joint Committee for Powder Diffraction standard, Card No. 84-0924
18. Chen Y-C, Lo G-M, Su M-Y (1996) Jpn J Appl Phys 35:2745
19. Langhammer HT, Müller T, Polity A, Felgner K-H, Abicht H-P (1996) Mater Lett 26:205
20. Lee B-K, Jung Y-I, Kang S-JL, Nowtony J (2003) J Am Ceram Soc 86:155
21. Brzozowski E, Castro MS (2004) J Eur Ceram Soc 24:2499
22. Ihring H (1978) J Phys C 11:819
23. Daniels J, Wernicke R (1976) Philips Res Repts 31:544
24. Kutty TRN, Murugara P (1985) J Mater Lett 3:195
25. Hari NS, Padmini P, Kutty TRN (1997) J Mater Sci Mater Elect 8:15
26. Hewang W (1961) Solid State Electron 3:51
27. Qi J, Chen W, Zhang Z, Tang Z (1997) J Mater Sci 32:713
28. Ali NJ, Milne SJ (1993) J Am Ceram Soc 76:2321
29. Ali NJ, Milne SJ J Mater Res (in press)
30. Illingsworth J, Al-Allak HM, Brinkman AW, Woods J (1990) J Appl Phys 66:2088
31. Miki T, Fujimoto A, Jida S (1998) J Appl Phys 83:1592